JCI insight

RESEARCH ARTICLE

The senescence-associated secretome as an indicator of age and medical risk

Marissa J. Schafer,[1,2] Xu Zhang,[1,2] Amanika Kumar,[3] Elizabeth J. Atkinson,[4] Yi Zhu,[1] Sarah Jachim,[1] Daniel L. Mazula,[1] Ashley K. Brown,[1] Michelle Berning,[1] Zaira Aversa,[1,2] Brian Kotajarvi,[5] Charles J. Bruce,[6] Kevin L. Greason,[7] Rakesh M. Suri,[7,8] Russell P. Tracy,[9] Steven R. Cummings,[10,11] Thomas A. White,[1] and Nathan K. LeBrasseur[1,2]

[1]Robert and Arlene Kogod Center on Aging, [2]Department of Physical Medicine and Rehabilitation, [3]Division Gynecologic Surgery, [4]Division of Biomedical Statistics and Informatics, Department of Health Sciences Research, [5]Center for Clinical and Translational Sciences, [6]Division of Cardiovascular Diseases, Department of Medicine, and [7]Division of Cardiovascular Surgery, Department of Medicine, Mayo Clinic College of Medicine, Rochester, Minnesota, USA. [8]Department of Thoracic and Cardiovascular Surgery, Cleveland Clinic Abu Dhabi, Abu Dhabi, United Arab Emirates and Cleveland, Ohio, USA. [9]University of Vermont, Burlington, Vermont, USA. [10]Department of Medicine, University of California, San Francisco, San Francisco, California, USA. [11]Research Institute, California Pacific Medical Center, San Francisco, California, USA.

Produced by senescent cells, the senescence-associated secretory phenotype (SASP) is a potential driver of age-related dysfunction. We tested whether circulating concentrations of SASP proteins reflect age and medical risk in humans. We first screened senescent endothelial cells, fibroblasts, preadipocytes, epithelial cells, and myoblasts to identify candidates for human profiling. We then tested associations between circulating SASP proteins and clinical data from individuals throughout the life span and older adults undergoing surgery for prevalent but distinct age-related diseases. A community-based sample of people aged 20–90 years (retrospective cross-sectional) was studied to test associations between circulating SASP factors and chronological age. A subset of this cohort aged 60–90 years and separate cohorts of older adults undergoing surgery for severe aortic stenosis (prospective longitudinal) or ovarian cancer (prospective case-control) were studied to assess relationships between circulating concentrations of SASP proteins and biological age (determined by the accumulation of age-related health deficits) and/or postsurgical outcomes. We showed that SASP proteins were positively associated with age, frailty, and adverse postsurgery outcomes. A panel of 7 SASP factors composed of growth differentiation factor 15 (GDF15), TNF receptor superfamily member 6 (FAS), osteopontin (OPN), TNF receptor 1 (TNFR1), ACTIVIN A, chemokine (C-C motif) ligand 3 (CCL3), and IL-15 predicted adverse events markedly better than a single SASP protein or age. Our findings suggest that the circulating SASP may serve as a clinically useful candidate biomarker of age-related health and a powerful tool for interventional human studies.

Introduction

Aging is the strongest risk factor for the majority of chronic diseases. Recent scientific advances have led to the transformative hypothesis that interventions targeting the fundamental biology of aging have the potential to delay, if not prevent, the onset of age-associated conditions and extend human health span (1). Notably, there is now compelling evidence that cellular senescence, a state of stable growth arrest caused by diverse forms of cellular and molecular damage, contributes to aging, in part, through the senescence-associated secretory phenotype (SASP) (2–4). Senescent cells accumulate with advancing age (5–7). Preclinical studies in rodents have established that transgenic strategies and drugs that selectively kill senescent cells improve numerous yet pathologically distinct conditions of aging, including idiopathic pulmonary fibrosis (8), cardiovascular disease (9, 10), hepatic steatosis (11), osteoporosis (12), diabetes (13), physical decline (14, 15), and brain dysfunction (16–18). Importantly, reducing SASP abundance and subsequent action is a likely mechanism by which senescent cell elimination improves aging conditions (8, 10, 19, 20). Consequently, there is great interest in human translation (21).

Dramatic variability is inherent to aging. Many older adults of a given chronological age experience multiple chronic conditions and functional limitations, while paired-age counterparts may have low or no disease bur-

Authorship note: MJS and XZ contributed equally to this work.

Conflict of interest: YZ and NKL have a financial interest related to this research. Patents on senolytic drugs are held by the Mayo Clinic (US20170216286A1). This research has been approved by the Mayo Clinic Conflict of Interest Review Board and was conducted in compliance with Mayo Clinic conflict of interest policies.

Submitted: September 20, 2019
Accepted: May 6, 2020
Published: June 18, 2020.

Reference information: *JCI Insight*. 2020;5(12):e133668. https://doi.org/10.1172/jci.insight.133668.

den and comparatively greater functional independence. Individuals with cumulatively more age-related impairments may be characterized as frail or biologically older according to a standardized accumulation-of-deficits index (22). Advanced biological age may be linked to a greater burden of senescent cells in one or multiple organs. Core properties of senescent cells include upregulation of cyclin-dependent kinase inhibitors, morphological changes, activation of antiapoptosis pathways, and a SASP composed of cytokines, chemokines, matrix remodeling proteins, and growth factors (23). Senescent cell properties can be quantified in isolated tissues; however, this poses practical challenges for human application. Since the SASP is a key pathogenic feature of senescent cells, leveraging the circulating SASP as an indicator of systemic senescent cell burden may offer considerable utility. In clinical research, it can help identify persons who may be most responsive to emerging therapies and serve as surrogate endpoints in associated clinical trials. In clinical practice, SASP quantification may identify persons of advanced biological age and guide clinical decision making. We hypothesize that SASP abundance may be associated with chronological aging and accelerated biological aging.

Herein, we sought to take advantage of the circulating SASP as a candidate biomarker of advanced age and/or medical risk. Based on the robust and dynamic SASP of several human cell types, we first established a candidate panel of 24 SASP proteins that can be reliably measured in human blood, and then studied associations with chronological age in a population-based sample of persons 20 to 90 years of age. We next examined associations between circulating SASP proteins and clinical manifestations of biological age using a frailty index (22) in 3 distinct cohorts of older adults. Finally, we assessed the extent to which circulating SASP factors predict adverse health outcomes after surgery for distinct age-related diseases.

Results

Senescent cells produce a robust and distinct SASP. To develop a candidate panel of SASP biomarkers for human application, conditioned media were collected from 5 senescent versus nonsenescent human cell types: endothelial and epithelial cells, preadipocytes, fibroblasts, and myoblasts. Irradiation-induced senescence was confirmed by senescence-associated β-galactosidase (SA–β-Gal) staining and real-time PCR analysis of senescence-activated genes (Figure 1A and Supplemental Figure 1; supplemental material available online with this article; https://doi.org/10.1172/jci.insight.133668DS1). A biased approach, based on the molecular knowledge of the SASP obtained in model systems, was used to select candidate proteins. High levels of both distinct and overlapping SASP factors, including cytokines, chemokines, matrix remodeling proteins, and growth factors, were identified in all senescent cells assayed relative to nonsenescent cells (Figure 1B and Supplemental Table 1). Senescent endothelial cells, preadipocytes, and fibroblasts produced a more robust SASP relative to epithelial cells and myoblasts, with distinct proteins increased per cell type (Figure 1, B and C; and Supplemental Tables 1 and 2). GDF15, OPN, and IL-8 were abundantly produced and secreted by senescent endothelial cells, whereas higher levels of IL-15, IL-6, PAI2, and ACTIVIN A were produced and secreted by senescent preadipocytes (Figure 1, B and C; and Supplemental Table 2). Thus, distinct cell types throughout the body may uniquely contribute to a dynamic SASP in vivo.

Circulating SASP factors are associated with advanced chronological age. Building on the premise that senescent cells accumulate with chronological age, the panel of 24 SASP proteins identified as biologically relevant in vitro was measured in the plasma of a random sample of 267 Mayo Clinic biobank participants (24). The sample was equivalently distributed by sex and age from 20 to 90 years (Supplemental Table 3). Circulating concentrations of 19 SASP proteins were associated with chronological age, and associations between 17 SASP factors and chronological age remained significant after adjusting for sex and BMI (Supplemental Table 4), highlighting the potential influence of sex and body composition on the biology of aging. Unadjusted Spearman's correlation analyses indicated that GDF15 and ACTIVIN A were the strongest candidate biomarkers of chronological age, followed by TNFR1, CCL4, FAS, CCL3, TNF-α, and IL-6, all of which individually explained at least 10% of the variance in chronological age (Figure 2). GDF15, ACTIVIN A, CCL4, FAS, CCL3, and TNF-α remained significantly associated with age after adjusting for sex and BMI (Supplemental Table 4).

Circulating SASP factors are associated with advanced biological age. The principal exploratory sample used to test associations between plasma levels of the panel of 24 SASP factors and biological age, as measured by the frailty index, was composed of older adults undergoing surgery for severe aortic stenosis ($n = 97$). To determine whether associations between biological age and circulating SASP factors were disease agnostic, plasma SASP factor concentrations were also assessed in a limited case-control study of older women undergoing surgery for ovarian cancer, in which women with a greater burden of age-associated deficits

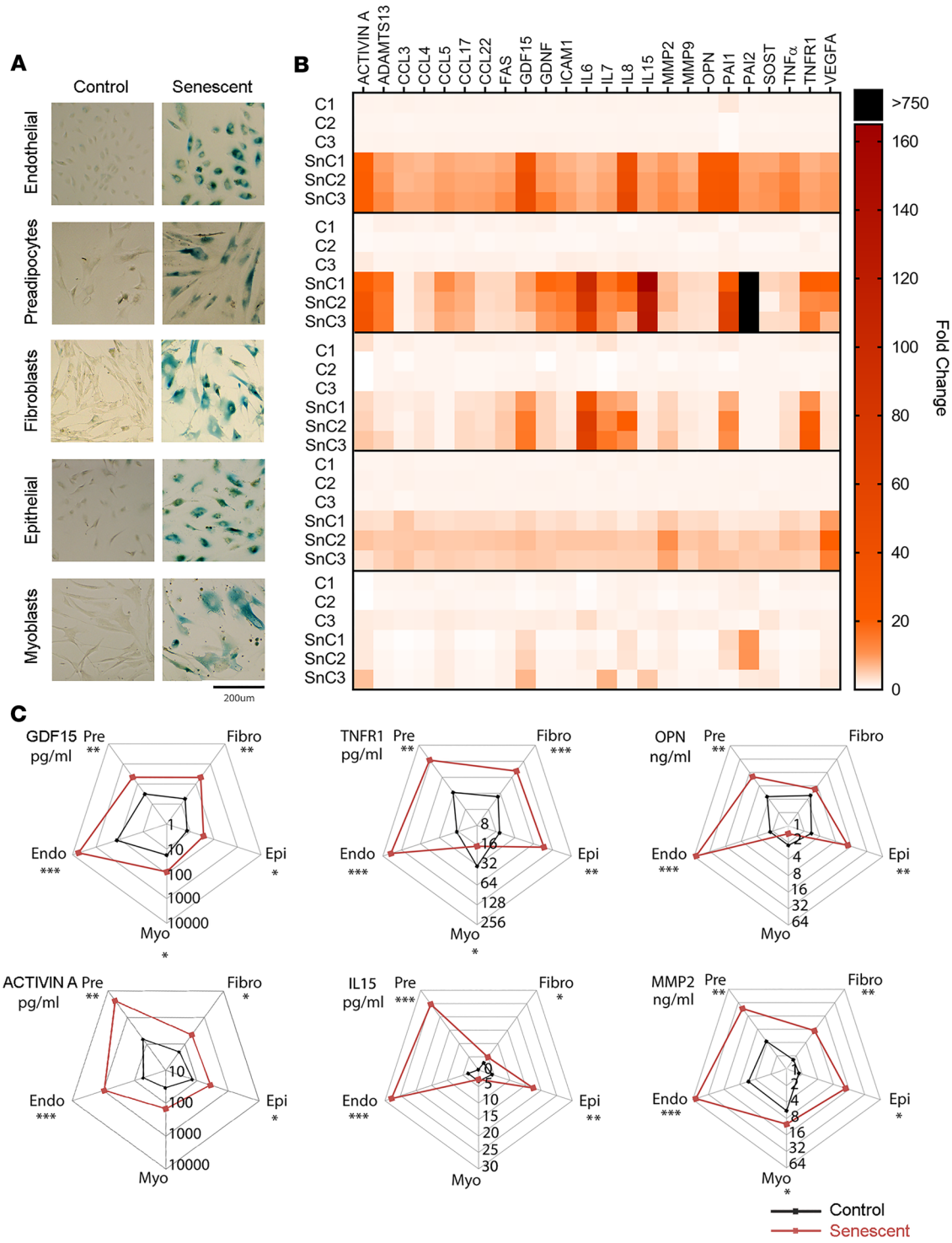

Figure 1. Senescent human cells secrete a heterogeneous SASP. (**A**) SA–β-Gal staining confirmed senescence induction in irradiated versus sham-treated human cells (scale bar: 200 μm). (**B**) Fold change in concentration of secreted SASP proteins by irradiated senescent cells (SnC) normalized to the sham control (C) samples for each cell type. (**C**) Absolute secreted protein concentration from 1 million senescent versus nonsenescent control cells. Abbreviations: endothelial cells (endo), preadipocytes (pre), fibroblasts (fibro), epithelial cells (epi), and myoblasts (myo). Mean is depicted; 2-tailed *t* tests with significance indicated as $^{*}P < 0.05$, $^{**}P < 0.01$, and $^{***}P < 0.001$; $n = 3$ replicates per cell type). See Supplemental Tables 1 and 2 for supportive data.

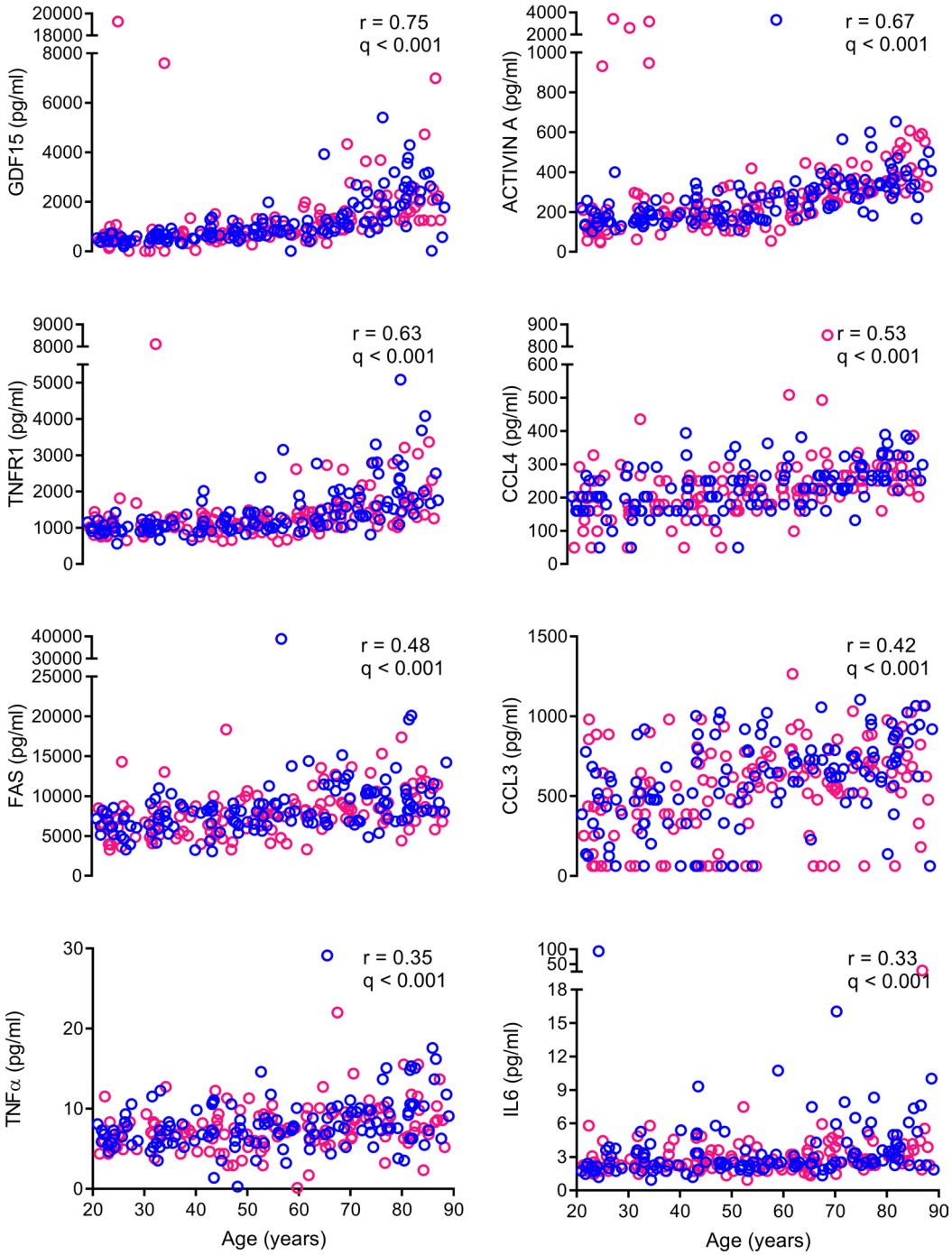

Figure 2. Circulating SASP factors are associated with chronological age. Circulating concentrations of SASP proteins demonstrating the strongest unadjusted FDR-corrected Spearman's correlations with chronological age are depicted among Mayo Clinic biobank participants age 20–90 years. Women (n = 137) are indicated by pink circles, and men (n = 130) are indicated by blue circles. See Supplemental Table 4 for supportive data.

based on the frailty index were compared with counterparts with lower deficit burden, yet of similar age and disease severity (n = 36). Plasma SASP factor concentrations and frailty index associations were also studied in the subset of 267 Mayo Clinic biobank sample participants age 60–90 years (n = 115). Demographic information for all 3 samples is presented in Supplemental Tables 5 and 6.

In unadjusted analyses, 8 SASP factors, ACTIVIN A, CCL4, GDF15, IL-6, IL-15, OPN, TNF-α, and TNFR1, were positively associated with the frailty index in any one of the 3 participant groups (Table 1;

Model 1). GDF15 and OPN increased in association with the frailty index in all 3 participant groups and remained significant after adjusting for chronological age, BMI, and/or sex as potential confounding or effect-modifying variables (Table 1). Similarly, after adjustment for age, BMI, and/or sex, TNFR1 was associated with a higher frailty index across all 3 groups. Increased CCL4 and TNF-α were associated with advanced biological age in both surgical groups and remained significant after adjustment, but were not significantly associated with the frailty index in aged, nonsurgical participants. IL-15 was positively associated with the frailty index in only the aortic stenosis and nonsurgical participant groups before and after adjustment. Using both unadjusted and adjusted models, ACTIVIN A and IL-6 were positively associated with the frailty index in the nonsurgical participants (Table 1).

Circulating SASP factors are associated with adverse postsurgical outcomes. Chronological age and biological age, as measured by the frailty index, are important predictors of adverse event risk following surgery (25, 26). Accordingly, relationships between presurgery circulating concentrations of SASP factors and adverse outcomes were examined in study participants who underwent surgery for severe aortic stenosis. Of 19 events assessed (myocardial infarction, new arrhythmia, new conduction abnormality, stroke, deep venous thrombosis, pulmonary emboli, pneumonia, plural effusion, new renal insufficiency, gastrointestinal bleeding, new seizure disorder, significant hypotension, significant tachycardia, significant bradycardia, urinary tract infection, other infection, acute dementia, vascular complication, acute kidney injury), 42 individuals had at least 1 adverse event (43% of participants) and 55 individuals had no adverse event within 12 months of hospital discharge. Participants experiencing at least 1 adverse event were of similar chronological age but had higher median frailty scores compared with participants with no adverse events (frailty index = 0.26 vs. 0.20, $P = 0.006$). Median circulating GDF15, OPN, MMP2, IL-15, and TNFR1 concentrations were significantly higher in participants with at least 1 adverse event compared with participants without adverse events (Figure 3A). As a predictor of risk of an adverse event within 12 months of surgery, the receiver operating characteristic AUC (ROC AUC) for GDF15 was 0.66; the ROC AUCs for frailty score and age plus sex were 0.65 and 0.56, respectively (Figure 3D).

Rehospitalization within 12 months of hospital discharge was assessed as a separate variable from any adverse event. Twenty-eight of the 97 participants undergoing surgery for severe aortic stenosis (29%) were rehospitalized within 1 year of surgical discharge. Participants who were rehospitalized at least once were of similar chronological age, but had advanced biological age compared with participants that were not (frailty index = 0.27 vs. 0.21, $P = 0.012$). Median circulating GDF15, TNFR1, FAS, and IL-6 concentrations were significantly higher among the rehospitalized versus nonrehospitalized participants (Figure 3B). The rehospitalization predictive ability of presurgery circulating GDF15, TNFR1, or IL-6 levels was equivalent to that of biological age (GDF15 ROC AUC = 0.66; TNFR1 ROC AUC = 0.66; IL-6 ROC AUC = 0.66; frailty index ROC AUC = 0.66) and potentially greater than the predictive ability of age plus sex (age + sex ROC AUC = 0.56) (Figure 3E).

In study participants who underwent surgery for ovarian cancer, the most common adverse event experienced was admission to the ICU within 30 days of surgery (12 of 36 total participants [33%]). Eight of the 12 individuals who were admitted to the ICU were frail cases and 4 were nonfrail controls, representing a nonsignificant relationship between frailty and ICU admission ($P = 0.157$). Median circulating levels of FAS, OPN, and ACTIVIN A before surgery were significantly higher among participants who were admitted to the ICU within 30 days of surgery relative to those who were not (Figure 3C). FAS, OPN, and ACTIVIN A were identified as the most robust candidate biomarker predictors of risk of an adverse event within 12 months of surgery, with potentially higher predictive power relative to either chronological age or biological age alone (FAS ROC AUC = 0.76; OPN ROC AUC = 0.74; ACTIVIN A ROC AUC = 0.74; age ROC AUC = 0.50; frailty index ROC AUC = 0.63) (Figure 3F).

Gradient boosting machine (GBM) modeling was next used to identify a single panel of SASP proteins capable of predicting adverse outcomes better than age or a single factor across the distinct aortic stenosis and ovarian cancer patient samples. A 7-protein panel consisting of GDF15, FAS, OPN, TNFR1, ACTIVIN A, CCL3, and IL-15 was consistently able to predict adverse events in both surgical populations more robustly than a single protein, biological age, or chronological age plus sex. Specifically, the ROC AUCs for discriminating risk of any adverse event or rehospitalization within 12 months of surgery for severe aortic stenosis were 0.84 and 0.81, respectively (Figure 3, D and E). The ROC AUC for discriminating risk of admission to the ICU within 30 days of surgery for ovarian cancer was 0.85 (Figure 3F).

Table 1. Circulating SASP factors are associated with biological age

		Aortic stenosis				Ovarian cancer				Referent, 60–90 years			
		Model 1		Model 2		Model 1		Model 3		Model 1		Model 2	
Protein	**Alias**	***r* value**	***q* value**	***r* value**	***q* value**	***r* value**	***q* value**	***r* value**	***q* value**	***r* value**	***q* value**	***r* value**	***q* value**
ACTIVIN A	INHBA	0.034	0.743	−0.066	0.352	0.226	0.301	**0.237**	**0.026**	**0.414**	**0.001**	**0.345**	**<0.001**
ADAMTS13	VWFCP	0.155	0.258	0.111	0.106	−0.028	0.911	−0.072	0.498	−0.020	0.954	0.038	0.647
CCL3	MIP1A, SCYA3	0.187	0.172	**0.187**	**0.005**	0.298	0.238	**0.316**	**0.003**	0.037	0.933	0.001	0.990
CCL4	MIP1B, SCYA4	**0.270**	**0.041**	**0.298**	**<0.001**	**0.495**	**0.012**	**0.530**	**<0.001**	0.214	0.144	0.139	0.065
CCL5	RANTES, SCYA5	0.167	0.217	**0.150**	**0.027**	0.213	0.301	**0.362**	**0.001**	−0.056	0.933	−0.083	0.278
CCL17	TARC, SCYA17	0.085	0.503	0.083	0.240	0.216	0.301	**0.284**	**0.005**	0.039	0.933	−0.031	0.682
CCL22	MDC, SCYA22	0.217	0.111	**0.144**	**0.030**	0.293	0.238	**0.321**	**0.002**	0.095	0.867	0.091	0.257
FAS	APT1, TNFRSF6	0.129	0.362	−0.026	0.712	0.269	0.270	**0.322**	**0.003**	0.076	0.912	0.029	0.682
GDF15	MIC1, NAG1, NRG1	**0.304**	**0.034**	**0.313**	**<0.001**	**0.490**	**0.012**	**0.344**	**0.001**	**0.369**	**0.002**	**0.333**	**<0.001**
GDNF	ATF	0.081	0.504	0.047	0.499	0.220	0.301	0.106	0.311	−0.069	0.912	−0.103	0.221
ICAM1	CD54	0.132	0.355	0.070	0.338	0.274	0.238	0.124	0.237	0.098	0.867	−0.047	0.550
IL-6	IFNB2	0.093	0.468	**0.207**	**0.001**	0.043	0.866	−0.203	0.054	**0.301**	**0.016**	**0.303**	**<0.001**
IL-7		0.113	0.409	0.061	0.390	0.231	0.301	**0.311**	**0.003**	0.014	0.954	−0.089	0.257
IL-8	CXCL8	0.166	0.217	−0.005	0.926	0.361	0.118	0.159	0.138	0.043	0.933	0.029	0.682
IL-15		**0.291**	**0.034**	**0.296**	**<0.001**	0.173	0.401	0.156	0.139	**0.279**	**0.028**	**0.280**	**<0.001**
MMP2	CLG4A	0.056	0.633	0.057	0.407	0.243	0.295	**0.363**	**0.001**	0.011	0.954	0.063	0.415
MMP9	CLG4B	−0.046	0.682	**−0.146**	**0.029**	−0.191	0.358	0.190	0.071	−0.015	0.954	0.124	0.112
OPN	SPP1, PSEC0156	**0.399**	**0.001**	**0.390**	**<0.001**	**0.489**	**0.012**	**0.354**	**0.001**	**0.314**	**0.013**	**0.365**	**<0.001**
PAI1	SERPINE1, PLANH1	0.117	0.402	0.106	0.112	0.126	0.567	**0.286**	**0.005**	−0.024	0.954	0.051	0.533
PAI2	SERPINEB2, PLANH2	0.188	0.172	**0.136**	**0.039**	0.063	0.805	**0.214**	**0.043**	−0.038	0.933	−0.080	0.283
SOST	DAND6	−0.105	0.441	**−0.151**	**0.027**	0.006	0.973	0.087	0.425	0.139	0.608	0.086	0.270
TNF-α	TNFSF2	**0.282**	**0.034**	**0.402**	**<0.001**	**0.499**	**0.012**	**0.413**	**<0.001**	0.090	0.867	0.067	0.396
TNFR1	CD120a	0.246	0.058	**0.263**	**<0.001**	**0.488**	**0.012**	**0.450**	**<0.001**	**0.375**	**0.002**	**0.359**	**<0.001**
VEGFA	VPH	0.249	0.058	**0.231**	**<0.001**	0.287	0.238	**0.308**	**0.004**	−0.006	0.956	−0.017	0.807

Model 1, FDR-corrected Spearman's correlation of frailty score versus protein concentration. Model 2, FDR-corrected Spearman's correlation of frailty score versus protein concentration adjusted for age, sex, and BMI. Model 3, FDR-corrected Spearman's correlation of frailty score versus protein concentration adjusted for age and BMI. Correlations of a significance level of $q < 0.05$ are shown in bold.

To explore the GBM-identified panel through another approach, we used t-distributed stochastic neighbor embedding (tSNE) projection to generate phenotypic participant clusters for circulating SASP factor comparisons. All participant samples in which frailty status was ascertained and all SASP proteins were measured were applied to this analysis (n = 343). The presence of any postoperative adverse event (any adverse event or rehospitalized within 12 months of surgery for the aortic stenosis group, ICU admission within 30 days of surgery for the ovarian cancer group), frailty score, and age were used as cluster definition variables (Supplemental Figure 2), rendering 6 clusters (Figure 3G). Clusters 1 and 2 consisted of nonfrail participants with no adverse events; cluster 1 was chronologically younger and cluster 2 was chronologically older. Clusters 3 and 4 consisted of participants with low to moderate frailty and no adverse events. Cluster 5 consisted of participants with higher frailty scores and adverse events, and cluster 6 consisted of participants with higher frailty scores and no adverse events. Scaled comparison of the GBM-identified 7-candidate biomarker panel (Figure 3H) revealed distinct profiles of SASP factor concentrations per cluster, with higher levels of GBM-identified SASP factors demarcating older, more frail adults who had an adverse event following surgery (cluster 5) from those who did not (cluster 6).

Discussion

Our findings demonstrated that distinct senescent cell types liberally secrete SASP proteins, with senescent endothelial cells, preadipocytes, and fibroblasts producing a more robust SASP relative to senescent epithelial cells and myoblasts. Components of the SASP can be reliably quantified in human plasma, and their circulat-

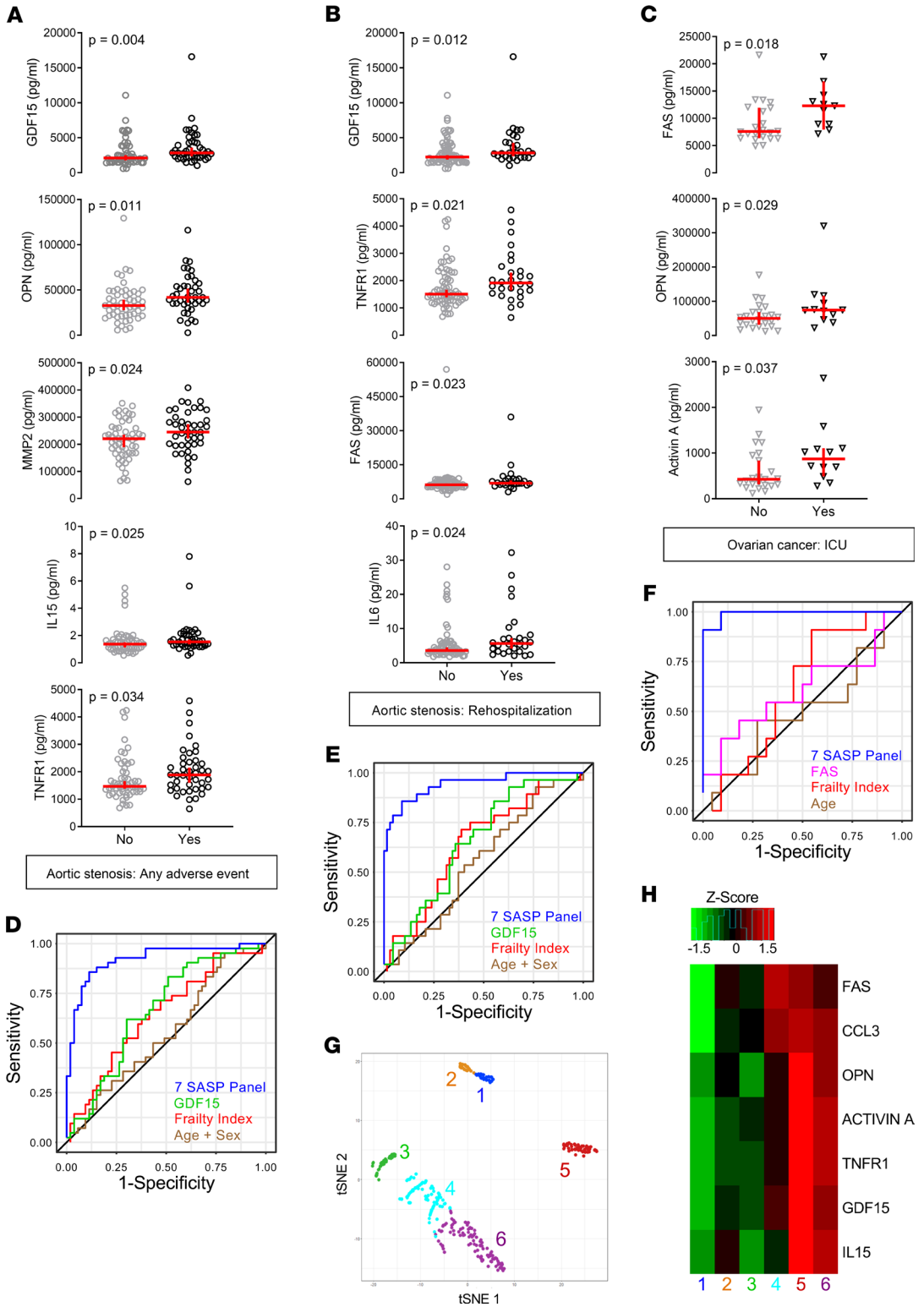
A
GDF15 (pg/ml)
p = 0.004
OPN (pg/ml)
p = 0.011
MMP2 (pg/ml)
p = 0.024
IL15 (pg/ml)
p = 0.025
TNFR1 (pg/ml)
p = 0.034
No
Yes
Aortic stenosis: Any adverse event
B
GDF15 (pg/ml)
p = 0.012
TNFR1 (pg/ml)
p = 0.021
FAS (pg/ml)
p = 0.023
IL6 (pg/ml)
p = 0.024
No
Yes
Aortic stenosis: Rehospitalization
C
FAS (pg/ml)
p = 0.018
OPN (pg/ml)
p = 0.029
Activin A (pg/ml)
p = 0.037
No
Yes
Ovarian cancer: ICU
D
Sensitivity
1-Specificity
7 SASP Panel
GDF15
Frailty Index
Age + Sex
E
Sensitivity
1-Specificity
7 SASP Panel
GDF15
Frailty Index
Age + Sex
F
Sensitivity
1-Specificity
7 SASP Panel
FAS
Frailty Index
Age
G
tSNE 2
tSNE 1
1
2
3
4
5
6
H
Z-Score
-1.5
0
1.5
FAS
CCL3
OPN
ACTIVIN A
TNFR1
GDF15
IL15
1
2
3
4
5
6

Figure 3. Circulating SASP factors are associated with increased risk of adverse postoperative outcomes. Levels of circulating SASP factors among older adults who underwent surgery for severe aortic stenosis and (**A**) experienced at least 1 adverse event (n = 42) or (**B**) were rehospitalized within 12 months of hospital discharge (n = 28) (black circles) were compared with counterparts who did not experience adverse outcomes (no adverse event, n = 55; no rehospitalization, n = 69) (gray circles). (**C**) Among older women who underwent surgery for ovarian cancer, circulating SASP factors were compared for participants who were admitted to the ICU within 30 days of surgery (n = 12) (black triangles) versus those who were not (n = 24) (gray triangles). (**A–C**: median ± 95% confidence interval are indicated with Kruskal-Wallis rank sum test results.) ROC AUCs indicating the adverse outcome risk discriminatory ability of a panel of 7 SASP factors (GDF15, FAS, OPN, TNFR1, ACTIVIN A, CCL3, and IL-15), a single top SASP factor (GDF15 or FAS), frailty score, or age plus sex for older adults undergoing surgery for (**D** and **E**) severe aortic stenosis or (**F**) age for older adults undergoing surgery for ovarian cancer. (**G**) All study participants in which accumulation of deficit frailty status was determined and all proteins were measured (n = 343) were clustered based on the presence of any postsurgical adverse event, frailty score, and chronological age. Six phenotypic clusters emerged: (1) nonfrail, younger, and no adverse events (n = 32); (2) nonfrail, older, and no adverse events (n = 25); (3) lower frailty score and no adverse events (n = 42); (4) intermediate frailty score and no adverse events (n = 82); (5) higher frailty score and adverse events (n = 53); (6) higher frailty score and no adverse events (n = 109). (**H**) Scaled concentration comparison of the 7 SASP proteins identified by GBM as associated with adverse events among the 6 clusters.

ing abundance significantly increases with chronological age. Consistent with findings in preclinical models showing the causative role of senescent cells in the pathogenesis of multiple age-related diseases and geriatric syndromes (8–18), higher circulating concentrations of SASP proteins were evident in older humans with more advanced biological age, as determined by accumulation of health and functional deficits. Among 2 samples of older adults undergoing surgery for distinct age-related diseases, individual SASP proteins showed predictive power for adverse postoperative events greater than chronological age, and greater than or equal to that of frailty index–defined biological age. Notably, a panel of 7 candidate biomarkers exhibited high sensitivity and specificity for adverse outcome risk prediction in participants undergoing surgery for either ovarian cancer or severe aortic stenosis. These results support the hypothesis that circulating SASP factors are informative candidate biomarkers of biological age that may be leveraged to predict risk for adverse health outcomes in a disease-agnostic manner, which may have wide relevance for clinical practice and clinical research.

The age-associated accumulation of DNA damage is a fundamental trigger for cellular senescence (27). Thus, we first implemented an in vitro screen to identify SASP proteins secreted in high concentrations by DNA damage–induced senescent cells relative to nonsenescent cells. Human endothelial and epithelial cells, preadipocytes, fibroblasts, and myoblasts, which develop pronounced age-related and/or senescent phenotypes in vivo, were selected for SASP profiling in vitro (8, 20, 28–32). This approach identified unique secretory phenotype composition and severity across cell types. In a translational context, these findings offer clues regarding the origin cells contributing to the SASP within the human circulating pool.

The differential contribution of distinct senescent cell types to the circulating SASP is likely dependent not only on the origin cell type, but also on the senescent induction mechanism and biophysical properties, such as proximity to the vasculature and protein chemistry. These complex parameters have thwarted in vivo characterization of the human SASP in the context of source cells; however, several studies have begun to characterize the transcriptomic and secretory phenotypes of senescent cells in distinct cellular contexts (19, 33–36). Findings derived from this study uniquely highlight the potential utility of SASP analyses for clinical application. For example, GDF15, which has an established role as a circulating factor that confers anorexia and cachexia (37), was strongly upregulated in DNA damage–induced senescent endothelial cells and fibroblasts. Higher circulating concentrations of GDF15 in participants of advanced chronological and biological age and at increased risk of adverse postsurgical outcomes suggest it may be a useful biomarker of age-related health. In contrast, PAI2 is a SASP factor with an established role in senescent cell survival (38) and was identified here to be a strongly upregulated SASP factor in senescent preadipocytes; however, comparatively weaker associations were identified between PAI2 and age or risk of adverse events, potentially limiting its usefulness as an informative circulating biomarker.

Analysis of circulating SASP proteins among older adults undergoing surgery for severe aortic stenosis or ovarian cancer and within a generalizable, nonsurgical sample of adults revealed distinct yet overlapping patterns corresponding to chronological versus biological age, as measured by the frailty index. These findings support the notion that chronological and biological aspects of aging are distinct, albeit highly related, and defined by unique biomarker signatures. Biological aging or frailty is intrinsically heterogeneous in that different forms of stress induce senescence in different cell types and confer subsequent functional decline. This heterogeneity supports the notion that a panel of SASP biomarkers may have broader utility in discriminating health risk across human populations, compared with a single biomarker with stress- or cell-type specificity. Here, a combination of 7 circulating SASP factors identified by GBM modeling was found to well-discriminate the risk of any adverse event and/or rehospitalization within 12 months of discharge among older adults

undergoing surgery for severe aortic stenosis or risk of admission to the ICU within 30 days of surgery among older women undergoing surgery for ovarian cancer. Using automated phenotypic clustering, we also demonstrated that increased abundance of the 7 SASP factor panel well-defined individuals who were biologically older and at greater risk of an adverse event. We highlight that the age-related conditions studied here are prevalent, but the pathogenesis of each disease is distinct, suggesting that the associations between the candidate biomarkers and health outcomes revealed here may have broad relevance.

The ability of the SASP to identify risk in other medical and surgical contexts warrants further investigation. The goal of our study was to establish a panel of SASP factors with reliable detection in human blood plasma or serum samples that are predictive of or associated with key clinical parameters and outcomes. Our current analyses were drawn primarily from residents of Olmsted County in Minnesota, so it is unclear whether our results are broadly generalizable. Although the factors identified demonstrated compelling associations with age and medical risk, our data also revealed the potential influence of other characteristics, including BMI and sex. Our study was not powered to explore the influence of these variables in depth, but these findings are important to consider, since women and men experience distinct risk profiles for age-related disease, and obesity is linked to a greater burden of senescent cells (39). Thus, there is great value in validating our findings and testing the generalizability of our panel in larger and more diverse groups of individuals with cardiovascular disease, cancer, and other age-associated conditions. Furthermore, an anticipated barrier to senescence-targeting clinical trials is a lack of readily quantifiable biomarkers that reflect biological age and health risk, and quantification of the SASP proteins analyzed herein may help identify persons who may be most responsive to senolytic therapeutics and may also serve as surrogate endpoints in clinical trials.

Methods

Cell culture experiments

Human fibroblasts (IMR90; ATCC) were cultured in DMEM containing 10% FBS and penicillin-streptomycin-glutamine (Gibco). Primary human preadipocytes isolated from 3 healthy kidney donors were cultured in α-MEM containing 10% FBS and penicillin-streptomycin-glutamine. HUVECs (Lonza,) were cultured in EGM-2 BulletKit (Lonza). Human epithelial cells (ARPE-19; ATCC) were cultured in DMEM/F12 containing 10% FBS and penicillin-streptomycin-glutamine. Human myoblasts derived from healthy donors (Cook MyoSite) were cultured in skeletal muscle cell growth medium (Promocell). Cells were exposed to sham conditions or, to induce senescence, 10 Gy radiation using an RS2000 X-Ray Irradiator (RAD Source Technologies). Fibroblasts, preadipocytes, epithelial cells, and myoblasts were then cultured for 21 days and HUVECs were cultured for 7 days before collection. Cells were provided fresh media every 3 days. After the indicated time, senescence was confirmed by staining for SA–β-Gal and real-time PCR analysis of cyclin-dependent kinase inhibitor (p16 and p21) and SASP gene expression. For SA–β-Gal staining, cells were fixed in phosphate-buffered 4% paraformaldehyde for 10 minutes at room temperature. Cells were then washed twice with PBS and incubated overnight (16–18 hours) in SA–β-Gal staining solution (1 mg/mL X-Gal, 40 mM citric acid/sodium phosphate buffer pH 6.0, 5 mM potassium ferrocyanide, 5 mM potassium ferricyanide, 150 mM sodium chloride, and 2 mM magnesium chloride) at 37°C on a shaker and in the dark. Cells were then washed twice with PBS and nuclei stained with Hoechst dye for 5 minutes. Fluorescence microscopy (Eclipse Ti) was used for imaging. Images were taken under bright field for SA–β-Gal staining and the same field under blue fluorescence channel for nuclear staining. Conditioned media from cultured fibroblasts, preadipocytes, myoblasts, and epithelial cells were obtained by exposing cells to RMPI 1640 containing 1 mM sodium pyruvate, 2 mM glutamine, MEM vitamins, MEM nonessential amino acids, and penicillin-streptomycin. Nonsenescent and senescent cells were washed 3 times with PBS and then cultured for 24 hours before media were collected. For HUVECs, cells were washed 3 times with PBS and then cultured in EBM-2 medium with 0.5% FBS for 24 hours before media were collected. Conditioned media were filtered through 0.22 μm filter before analysis. Cells were trypsinized, counted, and harvested in Trizol (Invitrogen) for RNA isolation according to the manufacturer's instructions. RNA concentration was assessed by NanoDrop (Thermo Fisher Scientific). cDNA was synthesized using M-MLV reverse transcriptase (Invitrogen), and real-time PCR was performed with PerfeCTa FastMix II (QuantaBio) and the Applied Biosystems StepOne Plus Real-Time PCR system. Gene expression was analyzed by delta-delta CT method and normalized to the reference gene, TATA-Box Binding Protein (TBP). The primers and probes used are listed in Supplemental Table 7.

Assessment of the SASP in biological fluids and cell culture media

The concentration of ADAMTS13, CCL3, CCL4, CCL5, CCL17, CCL22, FAS, GDF15, GDNF, ICAM1, IL-15, IL-6, IL-7, IL-8, MMP2, MMP9, OPN, PAI1, SOST, TNFR1, TNF-α, and VEGFA in conditioned media from nonsenescent and senescent cells and EDTA plasma were quantified using commercially available multiplex magnetic bead immunoassays (R&D Systems) based on Luminex xMAP multianalyte profiling platform and analyzed on a MAGPIX System (Merck Millipore). All assays were performed according to the manufacturer's protocols. ACTIVIN A concentration was determined by a Quantikine ELISA Kit (R&D Systems) according to the manufacturer's instructions. PAI2 concentration was determined by an ELISA Kit (Cloud-Clone Corp.) according to the manufacturer's instructions. For all proteins, more than 80% of the samples were within the detectable range. Undetectable targets were assigned a value of half of the lowest value; the number and percentage of imputed samples per target are summarized in Supplemental Table 8.

Participant samples

Biobank sample. The Mayo Clinic biobank is composed of residents of Olmsted County, Minnesota (n = 56,964) who donated biological specimens and provided risk factor data, access to clinical data obtained from the medical record, and consent to participate in approved research (24). The Mayo Clinic biobank started enrollment in April 2009. Participants were predominantly white (95%). For the present study, archived plasma samples were requested from 280 participants between 20 and 90 years of age (20 women and 20 men per decade). Participants with a history of cancer, other than breast cancer and melanoma, before the age of 50, or autoimmune diseases (e.g., rheumatoid arthritis, lupus), and women with BMI less than 18.5 kg/m^2 or greater than 40.0 kg/m^2 and men with BMI less than 18.5 kg/m^2 or greater than 35.0 kg/m^2 were excluded. Samples from 13 participants were of insufficient volume for SASP factor analysis, resulting in n = 267.

Aortic stenosis sample. This sample included women and men scheduled for surgical or transcatheter aortic valve replacement, as previously described (40, 41). Study participants were recruited between July 2013 and May 2015 at Mayo Clinic in Rochester, Minnesota. Demographic characteristics and medical history, including previous surgical events and diagnoses, were ascertained by interview, physical exam, and electronic medical record review at baseline. Adverse postoperative events were recorded 1, 3, 6, and/or 12 months after discharge from the hospital. For assessment of any adverse event within 12 months of discharge, the following outcomes were considered: myocardial infarction, new arrhythmia, new conduction abnormality, stroke, deep venous thrombosis, pulmonary emboli, pneumonia, plural effusion, new renal insufficiency, gastrointestinal bleeding, new seizure disorder, significant hypotension, significant tachycardia, significant bradycardia, urinary tract infection, other infection, acute dementia, vascular complication, or acute kidney injury. Rehospitalization within 12 months of discharge was considered as a separate adverse event.

Ovarian cancer sample. This sample included patients who underwent primary cytoreductive surgery for stage IIIC or IV ovarian cancer, fallopian tube cancer, or primary peritoneal cancer from January 2, 2003 to December 30, 2011. Exclusion criteria included patients who received neoadjuvant chemotherapy, patients undergoing palliative or diagnostic surgeries only, patients without a frailty index available, and patients who denied access to their medical record. All patients had a surgical resection to less than 1 cm of residual disease and all had a BMI less than 40 kg/m^2. Cases were defined as patients having a frailty index greater than 0.15. Cases were matched by age (within 3 years) and cancer stage to nonfrail controls.

Frailty index

The frailty index was calculated using a combination of comorbidities and patient-provided activities of daily living (ADL) variables abstracted from the medical record. The index reflects the percentage of variables that a given subject experienced. The comorbidity variables assessed were myocardial infarction, diabetes, peripheral vascular disease, chronic obstructive pulmonary disease, hypertension, hyperlipidemia, BMI (underweight/obese = 1 point, overweight = 0.5 points), anemia, cerebrovascular disease, dementia, peptic ulcer, hemiplegia/paraplegia, renal disease, moderate/severe liver disease, rheumatological disease, any malignancy, metastatic solid tumor, and depression. The ADL variables assessed were difficulty preparing meals, difficulty feeding oneself, difficulty dressing, difficulty using the toilet, difficulty housekeeping, difficulty climbing stairs, difficulty bathing, difficulty walking, difficulty using transportation, difficulty getting in and out of bed, difficulty taking medications/managing medications, dependent on assistive devices (cane, wheelchair, braces, walker, others), and dependent on device for breathing (CPAP, nasal oxygen).

Statistics

Two-tailed *t* tests were used to compare cell culture data. Descriptive statistics (percentages or medians/25th/75th percentiles and means/SD) were used to summarize the characteristics among patient cohorts. Comparisons between the groups were performed using χ^2 and Wilcoxon rank-sum tests. Spearman's correlation coefficients were used to summarize the relationship between the proteins and age. To account for multiple testing, false discovery rate values (*q* values) were calculated for each endpoint (42). Univariate logistic regression models were fit predicting adverse events using the candidate biomarker, age, sex, and frailty score variables; ROC AUCs were estimated from these models. GBM, a machine learning technique, was used to create a multivariable prediction model using the GBM package (43) available in the R software environment. This technique involves combining information from multiple decision trees that are iteratively built in such a way that each iteration focuses increasingly on the portions of the data that are most ill-fitting. The number of trees included in the model (number of iterations), the depth of the trees, and the size of the shrinkage parameter were determined by 5-fold cross-validation. AUC values from the GBM models were optimism corrected using an internal validation bootstrap process, since external data to validate the AUC values were not used (44). As part of the model results, variables were ranked in importance, indicating relative contribution to the models. tSNE clustering and phenograph analysis were performed using the cytofkit package (45). All other analyses were performed using SAS version 9.4 (SAS Institute), R 3.4.2 (R Foundation for Statistical Computing), R 3.6.0, or GraphPad Prism 8.1.2. Throughout all analyses, $P < 0.05$ or $q < 0.05$ were considered significant results.

Study approval

These studies were approved by the Mayo Clinic Institutional Review Board. All study participants provided written informed consent.

Author contributions

NL, MS, AK, TW, and XZ provided study design. NL, MS, XZ, AK, TW, EA, SJ, MB, ZA, BK, CB, KG, RS, DM, AB, YZ acquired, analyzed, or interpreted data. EA, MS, and XZ provided statistical analyses. MS, NL, AK, EA, XZ, and TW drafted the manuscript. BK, CB, KG, RS, SJ, ZA, RT, SC, and YZ provided critical revision of the manuscript. NL obtained funding.

Acknowledgments

This work was supported by the NIH, National Institute on Aging grants AG055529, AG060907, and AG044170 to NKL, the Glenn Foundation for Medical Research, Pritzker Foundation, Beverly Foundation, and Leonard and Mary Lou Hoeft Fund in Healthy Aging and Independent Living Research. We thank the Mayo Clinic Center for Individualized Medicine for providing access to Mayo Clinic biobank samples and data and Nino Giorgadze for providing human preadipocytes. We are grateful to Sabrina Brady for generating the graphical abstract.

Address correspondence to: Nathan K. LeBrasseur, Robert and Arlene Kogod Center on Aging, Mayo Clinic, 200 First Street SW, Rochester, Minnesota 55905, USA. Phone: 507.266.0727; Email: lebrasseur.nathan@mayo.edu.

1. Campisi J, Kapahi P, Lithgow GJ, Melov S, Newman JC, Verdin E. From discoveries in ageing research to therapeutics for healthy ageing. *Nature*. 2019;571(7764):183–192.
2. Muñoz-Espín D, Serrano M. Cellular senescence: from physiology to pathology. *Nat Rev Mol Cell Biol*. 2014;15(7):482–496.
3. LeBrasseur NK, Tchkonia T, Kirkland JL. Cellular Senescence and the Biology of Aging, Disease, and Frailty. *Nestle Nutr Inst Workshop Ser*. 2015;83:11–18.
4. van Deursen JM. The role of senescent cells in ageing. *Nature*. 2014;509(7501):439–446.
5. Dimri GP, et al. A biomarker that identifies senescent human cells in culture and in aging skin in vivo. *Proc Natl Acad Sci USA*. 1995;92(20):9363–9367.
6. Krishnamurthy J, et al. Ink4a/Arf expression is a biomarker of aging. *J Clin Invest*. 2004;114(9):1299–1307.
7. Geng YQ, Guan JT, Xu XH, Fu YC. Senescence-associated beta-galactosidase activity expression in aging hippocampal neurons. *Biochem Biophys Res Commun*. 2010;396(4):866–869.
8. Schafer MJ, et al. Cellular senescence mediates fibrotic pulmonary disease. *Nat Commun*. 2017;8:14532.
9. Roos CM, et al. Chronic senolytic treatment alleviates established vasomotor dysfunction in aged or atherosclerotic mice. *Aging Cell*. 2016;15(5):973–977.

10. Childs BG, Baker DJ, Wijshake T, Conover CA, Campisi J, van Deursen JM. Senescent intimal foam cells are deleterious at all stages of atherosclerosis. *Science*. 2016;354(6311):472–477.
11. Ogrodnik M, et al. Cellular senescence drives age-dependent hepatic steatosis. *Nat Commun*. 2017;8:15691.
12. Farr JN, et al. Targeting cellular senescence prevents age-related bone loss in mice. *Nat Med*. 2017;23(9):1072–1079.
13. Palmer AK, et al. Targeting senescent cells alleviates obesity-induced metabolic dysfunction. *Aging Cell*. 2019;18(3):e12950.
14. Xu M, et al. Senolytics improve physical function and increase lifespan in old age. *Nat Med*. 2018;24(8):1246–1256.
15. Baker DJ, et al. Naturally occurring p16(Ink4a)-positive cells shorten healthy lifespan. *Nature*. 2016;530(7589):184–189.
16. Musi N, et al. Tau protein aggregation is associated with cellular senescence in the brain. *Aging Cell*. 2018;17(6):e12840.
17. Bussian TJ, Aziz A, Meyer CF, Swenson BL, van Deursen JM, Baker DJ. Clearance of senescent glial cells prevents tau-dependent pathology and cognitive decline. *Nature*. 2018;562(7728):578–582.
18. Ogrodnik M, et al. Obesity-Induced Cellular Senescence Drives Anxiety and Impairs Neurogenesis. *Cell Metab*. 2019;29(5):1061–1077.e8.
19. Coppé JP, et al. Senescence-associated secretory phenotypes reveal cell-nonautonomous functions of oncogenic RAS and the p53 tumor suppressor. *PLoS Biol*. 2008;6(12):2853–2868.
20. Krtolica A, Parrinello S, Lockett S, Desprez PY, Campisi J. Senescent fibroblasts promote epithelial cell growth and tumorigenesis: a link between cancer and aging. *Proc Natl Acad Sci USA*. 2001;98(21):12072–12077.
21. Justice JN, et al. Senolytics in idiopathic pulmonary fibrosis: Results from a first-in-human, open-label, pilot study. *EBioMedicine*. 2019;40:554–563.
22. Searle SD, Mitnitski A, Gahbauer EA, Gill TM, Rockwood K. A standard procedure for creating a frailty index. *BMC Geriatr*. 2008;8:24.
23. Coppé JP, Desprez PY, Krtolica A, Campisi J. The senescence-associated secretory phenotype: the dark side of tumor suppression. *Annu Rev Pathol*. 2010;5:99–118.
24. Olson JE, et al. The Mayo Clinic Biobank: a building block for individualized medicine. *Mayo Clin Proc*. 2013;88(9):952–962.
25. Robinson TN, Wu DS, Pointer L, Dunn CL, Cleveland JC, Moss M. Simple frailty score predicts postoperative complications across surgical specialties. *Am J Surg*. 2013;206(4):544–550.
26. Orouji Jokar T, et al. Emergency general surgery specific frailty index: A validation study. *J Trauma Acute Care Surg*. 2016;81(2):254–260.
27. Hoeijmakers JH. DNA damage, aging, and cancer. *N Engl J Med*. 2009;361(15):1475–1485.
28. Zhou F, Onizawa S, Nagai A, Aoshiba K. Epithelial cell senescence impairs repair process and exacerbates inflammation after airway injury. *Respir Res*. 2011;12:78.
29. Bhayadia R, Schmidt BM, Melk A, Hömme M. Senescence-Induced Oxidative Stress Causes Endothelial Dysfunction. *J Gerontol A Biol Sci Med Sci*. 2016;71(2):161–169.
30. Xu M, et al. JAK inhibition alleviates the cellular senescence-associated secretory phenotype and frailty in old age. *Proc Natl Acad Sci USA*. 2015;112(46):E6301–E6310.
31. Sousa-Victor P, et al. Geriatric muscle stem cells switch reversible quiescence into senescence. *Nature*. 2014;506(7488):316–321.
32. Le Roux I, Konge J, Le Cam L, Flamant P, Tajbakhsh S. Numb is required to prevent p53-dependent senescence following skeletal muscle injury. *Nat Commun*. 2015;6:8528.
33. Rodier F, et al. Persistent DNA damage signalling triggers senescence-associated inflammatory cytokine secretion. *Nat Cell Biol*. 2009;11(8):973–979.
34. Coppé JP, et al. A human-like senescence-associated secretory phenotype is conserved in mouse cells dependent on physiological oxygen. *PLoS One*. 2010;5(2):e9188.
35. Özcan S, et al. Unbiased analysis of senescence associated secretory phenotype (SASP) to identify common components following different genotoxic stresses. *Aging (Albany NY)*. 2016;8(7):1316–1329.
36. Kuilman T, et al. Oncogene-induced senescence relayed by an interleukin-dependent inflammatory network. *Cell*. 2008;133(6):1019–1031.
37. Jones JE, et al. Supraphysiologic Administration of GDF11 Induces Cachexia in Part by Upregulating GDF15. *Cell Rep*. 2018;22(6):1522–1530.
38. Zhu Y, et al. The Achilles' heel of senescent cells: from transcriptome to senolytic drugs. *Aging Cell*. 2015;14(4):644–658.
39. Schafer MJ, et al. Exercise Prevents Diet-Induced Cellular Senescence in Adipose Tissue. *Diabetes*. 2016;65(6):1606–1615.
40. Schafer MJ, et al. Quantification of GDF11 and Myostatin in Human Aging and Cardiovascular Disease. *Cell Metab*. 2016;23(6):1207–1215.
41. Kotajarvi BR, et al. The Impact of Frailty on Patient-Centered Outcomes Following Aortic Valve Replacement. *J Gerontol A Biol Sci Med Sci*. 2017;72(7):917–921.
42. Benjamini Y, Hochberg Y. Controlling the false discovery rate: a practical and powerful approach to multiple testing. *J R Stat Soc Series B Stat Methodol*. 1995;57(1):289–300.
43. Ridgeway G. Generalized Boosted Models: A Guide to the GBM Package.R-Project. https://cran.r-project.org/web/packages/gbm/vignettes/gbm.pdf. Published January 14, 2019. Accessed May 18, 2020.
44. Steyerberg EW, Bleeker SE, Moll HA, Grobbee DE, Moons KG. Internal and external validation of predictive models: a simulation study of bias and precision in small samples. *J Clin Epidemiol*. 2003;56(5):441–447.
45. Chen H, Lau MC, Wong MT, Newell EW, Poidinger M, Chen J. Cytofkit: A Bioconductor Package for an Integrated Mass Cytometry Data Analysis Pipeline. *PLoS Comput Biol*. 2016;12(9):e1005112.